Journal of Science and Technology – Engineering and Technology for Sustainable Development
Volume 36, Issue 2, April 2026, 036–043

Effect of Synthesis Method of Ni/MgAlO$_x$ Catalyst in Dry Reforming of Methane: Initial Investigation

Tuong Huy Nguyen, Thanh Hung Nguyen, Dinh Hung Tran, Minh Thang Le*
Hanoi University of Science and Technology, Ha Noi, Vietnam
**Corresponding author email: thang.leminh@hust.edu.vn*

Abstract

The dry reforming of methane (DRM) is a promising route for converting greenhouse gases (CH_4 and CO_2) into valuable syngas (H_2 and CO), offering both environmental and economic benefits. Among the DRM catalysts in literature, nickel-based on hydrotalcite-derived material Ni/MgAlO$_x$ was chosen due to its catalytic activity and resistance to carbon residue and metal site agglomeration. The study presents an initial investigation into the effect of different synthesis methods on the physicochemical properties and catalytic performance of Ni/MgAlO$_x$ catalysts in DRM. The catalysts, with fixed Ni/Mg/Al ratio of 1.0/2.0/1.5, were synthesized using two different methods: a) co-precipitation with hydrothermal crystallization and b) sol-gel, to study how the differences in synthesis route can affect the catalytic properties and performance of each catalyst. Characterization techniques, including X-ray diffraction (XRD), temperature-programmed reduction (TPR), and scanning electron microscopy (SEM) were employed to analyze the catalysts. The results reveal that the synthesis method significantly impacts the Ni dispersion, metal-support interaction, and stability of the catalysts. Catalysts prepared via co-precipitation exhibited superior activity and stability, attributed to their enhanced Ni dispersion and stronger metal-support interaction. This work provides foundational insights into optimizing Ni/MgAlO$_x$ catalysts for DRM, highlighting the critical role of synthesis methods in tailoring catalytic performance.

Keywords: Dry reforming of methane, hydrotalcite, Ni/MgAlO$_x$, synthesis method.

1. Introduction

Fossil fuels continue to dominate global energy systems, leading to problems such as energy shortages and climate change. To resolve these issues, actions must be taken immediately, such as reducing CO_2 emissions and locating alternative, green, and sustainable energy sources. Additionally, modifying existing industrial processes or introducing new green processes can also be beneficial. Such measures not only contribute to environmental preservation but also pave the way for a more sustainable energy future.

One of the most promising chemical processes that can contribute to solving both CO_2 emission and energy shortage problem is the dry reforming of methane (DRM) reaction. Despite not being a novel concept, DRM has once again captured the attention of the scientific community due to its potential for addressing the energy shortage and climate change issue. The DRM process involves the catalytic conversion of two major greenhouse gases, methane (CH_4) and carbon dioxide (CO_2), into syngas, which is a mixture of hydrogen (H_2) and carbon monoxide (CO). Syngas is a highly versatile intermediate in the petrochemical industry, serving as building blocks for producing various valuable chemicals and fuels, such as methanol, ammonia, synthetic hydrocarbons through Fisch-Tropsch synthesis, etc. This dual purpose of DRM makes it an attractive strategy for sustainable energy and environmental management.

Unlike steam reforming of methane (SRM) and partial oxidation of methane (POM), DRM still cannot find its place in industrial applications. The main reason is the rapid deactivation of DRM catalysts, which are due to active sites sintering and coke accumulation caused by the following side reaction:

$$CH_4 + CO_2 = 2CO + 2H_2 \quad (\Delta H_{298K} = +247\ kJ/mol) \quad (1)$$

$$CH_4 = C + 2H_2 \quad (\Delta H_{298K} = +75\ kJ/mol) \quad (2)$$

$$2\ CO = CO_2 + C \quad (\Delta H_{298K} = -172.0\ kJ/mol) \quad (3)$$

$$CO_2 + H_2 = CO + H_2O \quad (\Delta H_{298K} = +41.0\ kJ/mol) \quad (4)$$

Carbon residue is mainly produced via reactions (2) and (3). Also, this reaction requires a high operating temperature (optimum temperature range of 870–1040 ^oC [1]) since the inert nature of CO_2 requires a high energy supply to activate, which is not beneficial and economical for an industrial process and also poses a risk of active sites agglomerating. Also, the operating pressure is a persistent problem, as it is not economical to run a gas phase reaction process at ambient pressure. Also, pressure in the range of 20 to 70 bars is recommended to join DRM with downstream processes [2], while 10 bars onwards favor the formation of solid surface coke and lower conversions [3]. Thus, there is an increasing need to developa catalyst that is stable

p-ISSN 3093-3242
e-ISSN 3093-3579
https://doi.org/10.51316/jst.189.etsd.2026.36.2.5
Received: Apr 24, 2025; Revised: Sep 7, 2025;
Accepted: Sep 15, 2025; Online: Mar 24, 2026

and active in harsh and long-term operations, to employ the process into practice.

DRM catalysts are bifunctional catalysts [4] that consist of active metal sites and support material. Among noble metals (Rh, Pt, etc.) and transition metals (Ni, Co), Ni was chosen due to its more reasonable price and availability, as well as its performance being comparable with that of noble metals [5]. Still, one of the drawbacks of Ni-based catalysts is the prohibition of carbon residue. In order to deal with the problem, several strategies can be employed, such as accumulated carbon species oxidation (by increasing basicity to attract CO_2 or introducing oxygen vacancies) or inhibiting the stabilization of coke by using bimetal alloys, etc. Many kinds of support material were researched: α-Al_2O_3 (conventional), hydrotalcite-derived material MgO-Al_2O_3 (basicity), perovskite, CeO_2, and/or ZrO_2 (oxygen storage). According to Papadopoulou *et al.* [6], among those catalysts, hydrotalcite-derived material has some unique properties that make it viable to use in DRM reaction, namely the basicity of MgO to attract CO_2 to oxidize both CH_4 and carbon residue. Also, its strong metal-support interaction can anchor the Ni active sites in place and prevent sintering effectively. Ha *et al.* [7] used La-Ni/$MgAlO_x$ catalyst to conduct DRM at the following reaction conditions: temperature of 750 ºC, a CH_4/CO_2 ratio of unity, and a severe gas hourly space velocity (GHSV) of 170 L/g_{cat}.h. Despite these harsh conditions, the catalyst achieved impressive CH_4 and CO_2 conversion of 80% and accumulated coke amount of only 0.77 wt. %. Meanwhile, Son *et al.* [8] tried to add MgO to their under-investigation material CoNi/γ-Al_2O_3 in an attempt to obtain $MgAl_2O_4$ phase. Using milder conditions: 850 ºC, $CH_4/CO_2/N_2$ equal to 1/1/1, GHSV of 40,000 h^{-1}, they obtained CH_4 and CO_2 conversion of about 95%, and surprisingly the sample withstood for 200 hours, which proved the potential of this kind of catalytic material. The combination of strong metal-support interaction, basicity, and resistance to carbon deposition makes hydrotalcite-derived materials a promising candidate for developing efficient and durable DRM catalysts.

Magnesium aluminate spinel ($MgAl_2O_4$) is a spinel oxide support extensively investigated in DRM. Under different calcination conditions, $MgAl_2O_4$ or MgO-Al_2O_3 mixtures would be formed [7]. $MgAl_2O_4$ offers a desirable combination of properties for ceramics due to its high melting temperature (2135 ºC), good chemical stability, and mechanical strength [9]. More importantly, various research confirmed the potential of this material [7–8, 10], as it has high activity, high durability, and all the advantages of the NiO-MgO solid solution mentioned above. Currently, Ni/$MgAl_2O_4$ catalyst is being used in some steam reforming (SRM) processes. Since the synthesis route can play a significant role in shaping catalyst properties and performance, this paper will emphasize using two well-known methods, a) co-precipitation followed by hydrothermal crystallization and b) the sol-gel method, to deeply understand how the synthesis route affects catalyst texture and performance. These methods are chosen for their ability to produce materials with distinct properties, allowing for a comprehensive comparison of how synthesis routes impact catalyst texture, metal-support interaction, and overall performance in DRM.

2. Materials and Methods

2.1. Catalyst Preparation

2.9835 g of $Ni(NO_3)_2.6H_2O$ was added to a 200 mL beaker, along with an appropriate amount of $Mg(NO_3)_2.6H_2O$ and $Al(NO_3)_3.9H_2O$ to achieve the desired metal molar ratio of Mg/Ni/Al equal to 2.0/1/1.5 (adapted from [11]). 70 mL of deionized water was added, and the metal nitrate precursors were mixed well and stirred continuously until reaching 70 ºC. In a separate beaker, 4.3512 g of NaOH pellets were well-stirred with 50 mL of deionized water. The obtained solution was then added dropwise under vigorous stirring at 70 ºC and 320 rpm until pH reached 11, at a rate of 1 mL per 10 s. The resulting suspension was aged for 1 hour at 70 ºC, then transferred into a 200 mL autoclave at 200 ºC for 24 h. After cooling to room temperature, the resulting suspension was filtered to separate the solid product. The collected solid was then washed thoroughly with deionized water under vacuum filtration until the washings reached a neutral pH of 7. The washed precipitate was dried overnight at 80 °C, followed by calcination at 850 °C for 6 hours. The obtained sample was named “NMA-ht”.

The amount of hydrated nitrate salts of metals in the sol-gel catalyst sample was also calculated so that the molar ratio of Mg/Ni/Al equal to 2.0/1/1.5. The nitrate solutions needed for the synthesis were prepared using the same amounts of salts as that of NMA-ht. The prepared metal nitrate solutions were put into a 250 mL glass beaker and magnetic stirred at 70 ºC for 1 hour on an electric stove. Then, citric acid monohydrate was added, providing that the solution had a molar ratio of citric acid to metal ions of 2.6. About 5 ml of concentrated HNO_3 was then added to prevent any precipitation reaction during the gelation process. Stirring speed and temperature was kept constantly at 70 ºC and 320 rpm to carry out the gelation process. The process continued until a clear gel was obtained. The gel was then dried at 150ºC for 5 hours. The resulting powder was then calcined at 500 ºC for 3 hours, and the obtained product was named “NMA-sg”.

2.2. Catalyst Characterization

X-ray diffraction (XRD) measurements of the catalyst samples were conducted using a Bruker D8 Advance instrument at the Department of Inorganic Chemistry, Hanoi University of Science. The analysis

was performed under the following conditions: Cu Kα radiation with a wavelength (λ) of 0.15406 nm, a scanning angle (2θ) range of 20° to 80°, and a scanning rate of 0.02° per second. This technique was employed to investigate the crystallographic structure, phase composition, and crystallite size of the catalysts, providing critical insights into the influence of the synthesis method on the material's structural properties.

For morphology and surface elemental analysis, field emission scanning electron microscopy (SEM) and energy-dispersive X-ray spectroscopy (EDS) were carried out using a JCM–7000 NeoScopeTM Benchtop instrument (Japan), available at the GeViCat Center, Hanoi University of Science and Technology. The SEM measurements enabled high-resolution imaging of the catalyst surface, revealing details about particle size, morphology, and distribution, while the integrated EDS detector facilitated elemental mapping and surface compositional analysis. These combined techniques provided a comprehensive understanding of the catalyst's microstructure and elemental distribution so that the correlation between the synthesis method and catalytic performance can be confirmed. Practically, since EDS measurements can be influenced by factors such as sample heterogeneity, surface roughness, and the distribution of elements within the analyzed area, performing multiple attempts and averaging the results helps to mitigate these variations.

The temperature-programmed reduction with hydrogen (TPR – H_2) characterization was performed using an AutoChem II 2920 V5.02 (Micromeritics, USA) at GeviCat Center, Hanoi University of Science and Technology. Each time, 100 mg of a sample was loaded inside a U-shape quartz reactor and treated at 300 °C for 1 hour (10 °C/min, in 50 mL/min He flow) to remove adsorbed species in the sample pores. After the system cooling to 50 °C, a 10% H_2/Ar gas mixture (30 mL/min rate) was used to reduce the sample. This analytic process was conducted while the temperature was increased from 25 °C to 900 °C at a heating rate of 10 °C/min, monitored using a thermal conductivity detector (TCD).

2.3. Catalytic Test

DRM was conducted inside a fixed-bed quartz reactor (inner diameter of 2 mm, length of 50 cm) at 750 ºC under ambient pressure and GHSV of 15 L/(g_{cat}.h). Gas flow controllers (GFCs) model GFC 17-AALBORG were used to supply the feed gases and control the feed flow accurately. GFCs calibration, GC calibration, and peak identification were done using standard gas bottles of varying concentration. The feed gas was mixed using a mixture of 35 vol.% CH_4 in N_2 and 99.9 vol.% CO_2 to reach the feed ratio of $CH_4/CO_2/N_2$ equal to 1/1/2. All volumetric flow rates in this study are defined at normal temperature and pressure (NTP). In each experiment, 200 mg of catalyst (particle size from 200 to 450 μm) was put inside the reactor, and reaction temperature was input and displayed by a temperature controller connected to the electrical furnace (Nabertherm Controller model B170). Before each test, *ex-situ* catalyst reduction was carried out with a TPR-H_2 apparatus using 50 mL/min of pure H_2 at 700 °C for 1 h. Outlet gas composition was determined using an on-line gas chromatograph (Trace GC Ultra – Thermo Scientific) with a flame ionization detector (FID) and TCD as detectors.

3. Results and Discussion

3.1. Catalyst Characterization

Morphology and surface elemental analysis

Fig. 1a shows that the NMA-ht material tends to form large, leaf-like aggregates with a rough and uneven surface texture. At higher magnification (×8000, Fig. 1b), it can be observed that these leaf-like structures are actually made up of smaller, rod-shaped particles. These rods cluster together into larger blocks, creating a porous, cotton-like structure. On the other hand, the sol-gel sample looks completely different, showing a flake-like shape with a much smoother surface, as seen at the same magnification (x8000). The smoothness of the sol-gel material suggests a more uniform and controlled formation process, which is typical for sol-gel synthesis. These differences in morphology highlight how the synthesis method plays a key role in shaping the final structure of the material, which could have a significant impact on its catalytic properties and performance.

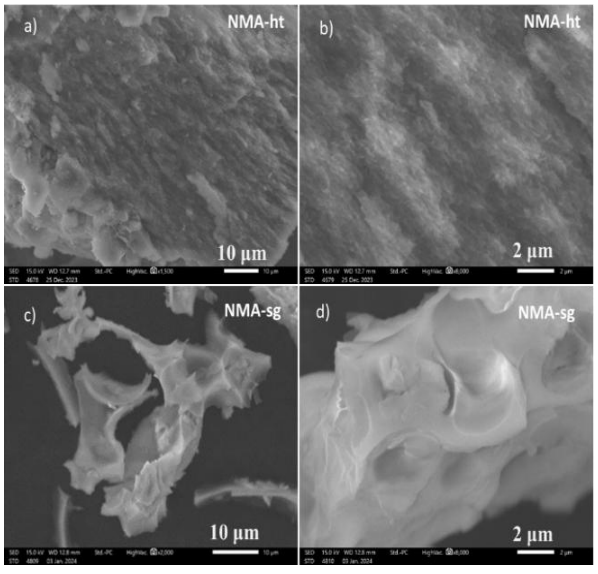

Fig. 1. SEM images of NMA-ht and NMA-sg

The EDS elemental results (Table 1) revealed that NMA-ht has the Ni:Mg:Al ratio closer to the target ratio of 1.0:2.0:1.5, suggesting a relatively successful incorporation of the desired elements during the synthesis. Meanwhile, the result of NMA-sg indicated

potential Ni loss during the preparation of this catalyst, considering the Mg/Al actual ratio of this sample (4.7/3.7) was aligned well with the desired ratio (2.0/1.5). In other words, the sol-gel method effectively maintained the Mg and Al composition but struggled to retain Ni.

Table 1. Element composition of the NMA samples by EDS

Sample	Element	Molar %	Molar ratio	Target molar ratio
NMA-ht	Ni	6.2	1.0	1.0
	Mg	8.8	1.4	2.0
	Al	13.6	2.2	1.5
	O	71.4	-	-
NMA-sg	Ni	4.3	1.0	1.0
	Mg	20.1	4.7	2.0
	Al	15.8	3.7	1.5
	O	58.8	-	-
Spent NMA-ht	C	14.8		
	Ni	12.3		
	Mg	11.5		
	Al	20.6		
	O	40.8		
Spent NMA-sg	C	66.8		
	Ni	2.1		
	Mg	5.2		
	Al	5.7		
	O	20.2		

For NMA-ht, even though the result matched better, a minor loss of Mg still could be observed, which could be attributed to partial leaching or incomplete incorporation during synthesis. The EDS data also indicated that NMA-ht contains higher Ni content compared to NMA-sg. This difference suggests that NMA-sg might exhibit better Ni dispersion and potentially smaller Ni particle sizes, as the lower Ni content could be ascribed to a more uniform distribution of Ni across the catalyst surface. Thus, EDS gave an initial insight into how the outcome of the two synthesis methods differs.

Elemental mapping was also employed to study the surface distribution of elements. Fig. 2 presents the elemental mapping results of the NMA samples. A uniform distribution of Mg, Al, and O was detected across the surface of both catalysts. However, the distribution of Ni showed notable differences between the two samples. Contrary to the initial assumption that NMA-ht might exhibit poorer Ni dispersion due to its higher overall Ni content, the elemental mapping demonstrated that Ni was actually more evenly distributed on the surface of NMA-ht compared to NMA-sg. Therefore, it is likely that there were other factors affecting Ni dispersion of the NMA catalysts. The distribution of Ni is a vital factor in determining the catalytic performance of these materials, as uneven Ni distribution can lead to the formation of Ni clusters or bulk particles, which reduce surface area and limit the number of accessible active sites.

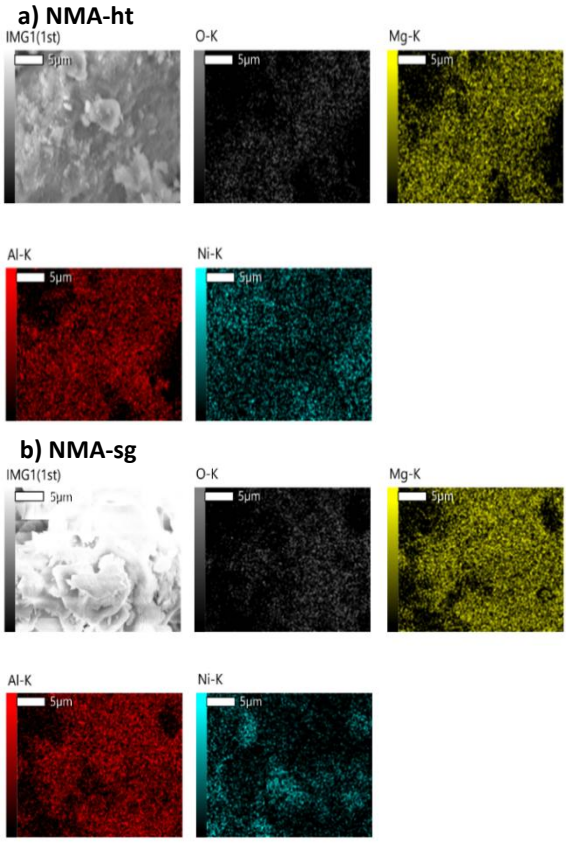

Fig. 2. Elemental mapping graphs of a) NMA-ht and b) NMA-sg

Crystallinity and reducibility

Fig. 3. shows the XRD results of freshly calcined samples (not reduced) and one spent sample of NMA-sg. The obtained XRD diffractograms were compared with International Centre for Diffraction Data (ICDD) database of cubic spinel $MgAl_2O_4$ (ICDD: 00–021-1152, main maxima at 2θ of 19.0º (111), 31.3º (220), 36.9º (311), 44.8º (400), 59.4º (511), and 65.2º (440), periclase MgO (ICDD 01-076-2583, main maxima at 2θ of 36.9º (111), 42.9º (200), 62.3º (220), 74.7º (311), and 78.6º (222), NiO (ICDD: 01-075-0269, main maxima at 2θ of 37.3º (111), 43.3º (200), 62.9º (220), 75.4º (311), and 79.4º (222)), and γ-Al_2O_3 (ICDD: 01-079-1558, main maxima at 2θ of 19.4º (111),

32.0º (220), 37.7º (311), 45.8º (400), 59.4º (511), and 66.8º (440).

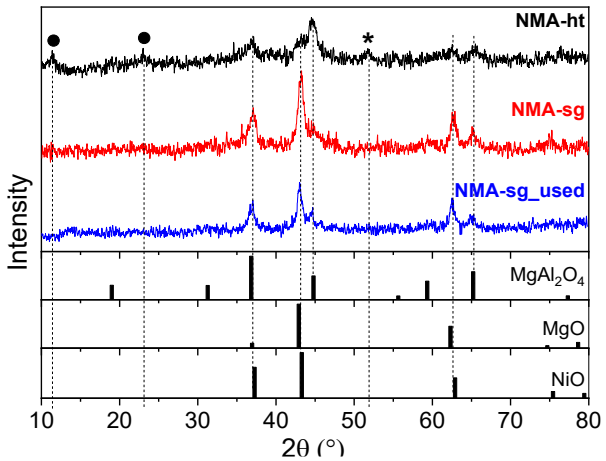

Fig. 3. XRD Diffractograms of NMA-ht, NMA-sg, and spent NMA-sg. (•) hydrotalcite structure according to [12]. The (*) reflection may suggest the presence of Ni phase (ICDD 00-004-0850, main maxima at 2θ of 44.5º and 51.9º)

According to the obtained XRD diffractograms, NMA-ht shows distinct diffraction of $MgAl_2O_4$, while NMA-sg has MgO and NiO signature maxima, which cannot be distinguished due to maxima overlap. González *et al.* [13] also investigated sol-gel Ni/$MgAlO_x$ catalysts and obtained the same results: their samples also have signature maxima of NiO (at 37.3º, 43.3º, 62.9º, and 75.4º). No γ-Al_2O_3 reflections were detected in any of the samples, possibly due to high loadings of MgO and NiO, or $MgAl_2O_4$ formation was favored over γ-Al_2O_3 [14]. After calcination, NMA-ht still retained its hydrotalcite characteristic peaks (at 2θ of 11° and 23°), which are supposed to disappear due to the collapse of the lamellar structure during calcination [12-13]. Considering the dominance of MgO and NiO signals in NMA-sg reflections, it can be inferred that MgO and NiO large bulks were formed within this sample, while NMA-ht has mainly $MgAl_2O_4$ structure indicated by the domination of $MgAl_2O_4$ reflections. In other words, NiO dispersion of NMA-ht is better, which agrees well with the elemental mapping results. Thus, it can be anticipated that poor distribution (or bulks/cluster forming) of Ni on the surface of NMA-sg can badly disrupt the catalytic activity of the sample.

Comparing to NMA-sg, used NMA-sg still keeps all the distinct maxima and only experiences a slight decrease in peak intensity.

The H_2-TPR profile (Fig. 4.) showed the signals of the two NMA samples, as well as their total H_2 consumption. The slight difference (approximately 10%) in H_2 consumption may suggest Ni loss over the samples in which NMA-sg experienced more loss, as shown in Table 1 and discussed above. The two signals both indicated two prominent peaks, one in the temperature range of 400–600 ºC (the α range) and the other one in the range of over 600 ºC (the β range). Meanwhile, fresh NiO samples only show a single maximum at 400 ºC [14, 15]. Additionally, it is mandatory to know that MgO and Al_2O_3 cannot be reduced at this experiment condition, as only NiO and maybe some surface hydroxyl and oxygen species are reducible, according to Özdemir *et al.* [16]. Therefore, such changes in the number of peaks and maxima suggest the reduction of the NiO interacted with MgO species. According to Guo *et al.* [15], for NiMgAl catalysts, the temperature range of 400–600 ºC characterizes the reduction of the surface NiO, which has little interaction with MgO or $MgAl_2O_4$ particles. Conversely, the temperature range exceeding 600 ºC indicates the reduction of NiO strongly interacted with the support. In NMA-ht's case, it shows only one small maximum in α range (at 411 ºC), as all its major reduction peaks shift towards β range, which accounts for the NiO's strong interaction with the support.

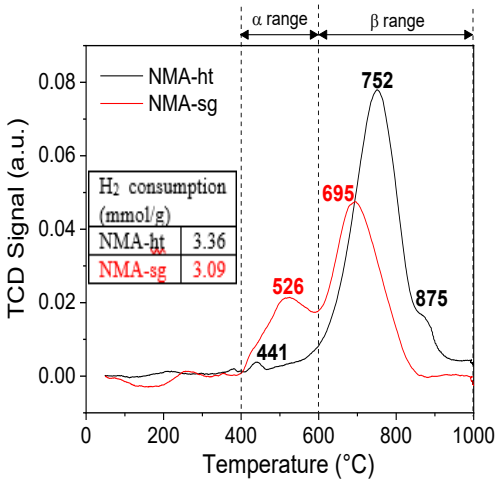

Fig. 4. H_2-TPR profile of NMA-ht and NMA-sg

Meanwhile, NMA-sg has an α peak at 526 ºC and a β peak at 695 ºC. The α peak is much larger in peak area than that of NMA-ht, while the β peak is smaller than the β peak (at 752 ºC) of NMA-ht. Considering that H_2 consumption links directly to NiO species, it can be inferred that NMA-sg has more NiO species in α range and less in β range than NMA-ht. This finding proved that NiO species in NMA-ht have stronger metal-support interaction than the ones in NMA-sg. According to the authors [6], strong metal-support interaction is beneficial for the catalyst system because it helps the Ni particles to disperse finely and anchors them in place to avoid sintering at high operating temperatures.

Last but not least, the shoulder at 875 ºC can be interpreted as the reduction of Ni species in $NiAl_2O_4$ spinel, as Özdemir *et al.* [16] stated in their work. Early studies claimed that apart from $MgAl_2O_4$, spinel $NiAl_2O_4$ can also be formed [4, 17, 18], which is a kind

of Ni species that has even stronger interaction with the support (TPR-H_2 maxima at 875 °C). It is sometimes known as "inactive" species, likely due to the fact that most DRM experiments were conducted at 600–800 °C, so it is nearly impossible to reduce. Thus, it is recommended to avoid the formation of spinel $NiAl_2O_4$ in order to avoid losing Ni active sites by forming inactive domains.

Therefore, it can be concluded from H_2-TPR results that Ni active sites dispersion on NMA-ht is significantly better compared to NMA-sg, which is also proved and discussed using elemental mapping and XRD results above. Consequently, it can be anticipated that NMA-ht might exhibit superior performance in catalytic tests compared to NMA-sg. On the other hand, with more NiO species in α range than NMA-ht, which translates into having weaker interaction with the support, NMA-sg is more prone to sintering and coke accumulation, knowing that it has poor Ni dispersion and tends to form large bulks and clusters.

Catalytic Activity

DRM was performed at 750 °C for 2 hours with $CH_4/CO_2/N_2$ feed composition of 1:1:2 and GHSV of 15 L/(g_{cat}·h). Fig. 5. shows that the two samples followed different pathways. NMA-ht went through an induction period (from the 20th to the 80th minute) and then stabilized at almost 100% CH_4 conversion. Such an induction period can be explained by considering the properties of the reaction. Since the reaction took place at 750 °C and in the presence of CO and H_2 (which can also act as reducing agents), the catalyst can be fully reduced and activated. On the other hand, there was no activity of NMA-sg. Although lower Ni content may increase dispersion [7], the structure formation ($MgAl_2O4$ or NiO bulks/clusters) is the key factor determining the catalytic activity, which was determined by the synthesis method. Considering all the characterization results, it is of high probability that the catalyst was deactivated due to active sites sintering. It was mentioned earlier that NMA-sg is susceptible to active sites sintering and coking due to poorer Ni distribution and weaker interaction with the support compared to NMA-ht. Moreover, since the Tammann temperature (the temperature at which crystal migration phenomena occur) of Ni is 691 °C [19], and considering how poorly Ni distributed on NMA-sg even before conducting catalytic test, the assumption was probably correct, as NMA-sg suffered from severe sintering.

To further investigate the cause of deactivation of NMA-sg catalyst, EDS analysis was performed on two spent catalyst samples: spent NMA-ht and spent NMA-sg, with all EDS points taken on the material surface in order to focus solely on carbon deposition. The resulting, summarized in Table 1, revealed significant differences in the extent of coke formation between the two catalysts. Specifically, the surface of NMA-sg exhibited a substantial accumulation of coke, with a carbon content of 66.8%, compared to only 14.8% on the surface of NMA-ht. This pronounced difference in coke deposition was accompanied by a corresponding decrease in the metal content on the surface of NMA-sg, suggesting that carbonaceous species heavily covered the active sites. The extensive coke formation on NMA-sg is likely the primary reason for its rapid deactivation, as the carbon deposits physically block the active sites, preventing reactant access and hindering catalytic activity.

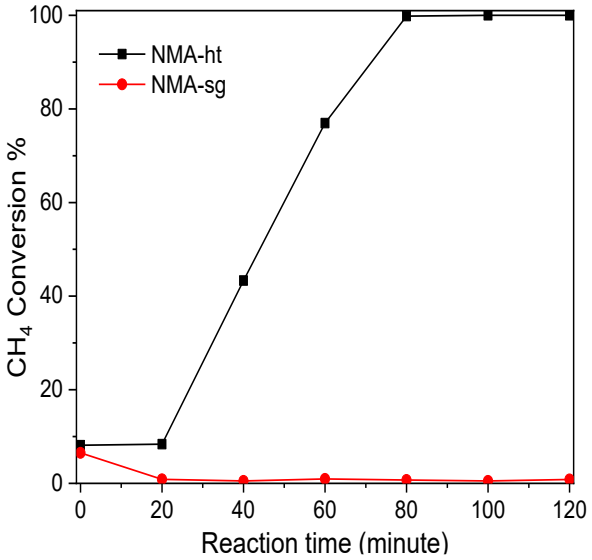

Fig. 5. CH_4 conversion of the two NMA catalysts against reaction time. Reduction conditions: 1 h, 700 °C, 50 mL/min H_2. Reaction conditions: $CH_4/CO_2/N_2$ = 1:1:2, T = 750 °C, m_{cat} = 200 mg, GHSV = 15 L/(g_{cat}·h)

In contrast, the relatively lower coke content on NMA-ht indicates better resistance to carbon deposition, which correlates with its sustained performance over time. The contrast in coke accumulation between the two catalysts provides a plausible explanation for the observed deactivation of NMA-sg after only 20 minutes of time-on-stream (TOS). These findings, along with the characterization results above, highlight the importance of designing catalysts with both enhanced resistance to carbon deposition and metal agglomeration for improved stability and longevity in the DRM process.

4. Conclusion

$Ni/MgAlO_x$ catalysts (NMA-ht and NMA-sg) were synthesized using co-precipitation method with hydrothermal crystallization and sol-gel method, respectively, and had catalytic properties and performance investigated. This initial investigation into the effect of synthesis methods on Ni/MgAlOx catalysts for the dry reforming of methane (DRM) has demonstrated that the preparation approach significantly influences the structural, morphological, and catalytic properties of the materials. Through comprehensive

characterization using XRD, SEM-EDS, and H_2-TPR, it was revealed that the synthesis method impacts Ni dispersion and metal-support interaction, thus affecting catalyst performance and stability. Catalysts prepared via co-precipitation, with the formation of $MgAl_2O_4$ phase, exhibited superior performance in terms of activity and stability due to their enhanced Ni dispersion and stronger interaction with the $MgAlO_x$ support. In contrast, catalysts synthesized by sol-gel methods, with the formation of NiO-MgO large bulks, showed poor performance, highlighting the importance of strong metal-support interaction to the durability of DRM catalysts. The findings confirm the role of the synthesis method in tailoring the physicochemical properties of $Ni/MgAlO_x$ catalysts for DRM. This study provides a fundamental understanding of how different preparation techniques influence catalyst behavior, which can guide future optimization efforts. Overall, this work contributes to the growing body of knowledge on catalyst design for greenhouse gas conversion and highlights the potential of $Ni/MgAlO_x$ catalysts in attempts to industrialize DRM process and head towards a sustainable future.

Acknowledgments

This research has been facilitated and assisted at GeViCat Laboratory, Hanoi University of Science and Technology, which is established by the RoHan Project funded by the German Academic Exchange Service (DAAD, No. 57315854) and the Federal Ministry for Economic Cooperation and Development (BMZ) inside the framework "SDG Bilateral Graduate School programme".

References

[1] S. Wang, G. Q. (Max) Lu, and G. J. Millar, Carbon dioxide reforming of methane to produce synthesis gas over metal-supported catalysts: State of the art, Energy and Fuels, vol. 10, iss. 4, pp. 896–904, Jul. 1996. https://doi.org/10.1021/ef950227t

[2] Linus A. Schulz, Lea C. S. Kahle, Karla Herrera Delgado, Stephan A. Schunk, Andreas Jentys, Olaf Deutschmann, and Johannes A. Lercher, On the coke deposition in dry reforming of methane at elevated pressures, Applied Catalysis A: General, vol. 504, pp. 599–607, Sep. 2015. https://doi.org/10.1016/j.apcata.2015.03.002

[3] E. le Saché and T. R. Reina, Analysis of dry reforming as direct route for gas phase CO_2 conversion. The past, the present and future of catalytic DRM technologies, Progress in Energy and Combustion Science, vol. 89, Mar. 2022, Art. no. 100970. https://doi.org/10.1016/j.pecs.2021.100970

[4] B. Abdullah, N. A. Abd Ghani, and D. V. N. Vo, Recent advances in dry reforming of methane over Ni-based catalysts, Journal of Cleaner Production, vol. 162, pp. 170–185, Sep. 2017. https://doi.org/10.1016/j.jclepro.2017.05.176

[5] Z. Hou, P. Chen, H. Fang, X. Zheng, and T. Yashima, Production of synthesis gas via methane reforming with CO_2 on noble metals and small amount of noble-(Rh-) promoted Ni catalysts, International Journal of Hydrogen Energy, vol. 31, no. 5, pp. 555–561, Apr. 2006. https://doi.org/10.1016/j.ijhydene.2005.06.010

[6] C. Papadopoulou, H. Matralis, and X. Verykios, Utilization of biogas as a renewable carbon source: Dry reforming of methane, in Catalysis for Alternative Energy Generation, New York, US: Springer, 2012, ch. 3, pp. 57–127. https://doi.org/10.1007/978-1-4614-0344-9_3

[7] Q. L. M. Ha, U. Armbruster, C. Kreyenschulte, H. Atia, H. Lund, H. T. Vuong, and S. Wohlrab, Stabilization of low nickel content catalysts with lanthanum and by citric acid assisted preparation to suppress deactivation in dry reforming of methane, Catalysis Today, vol. 334, pp. 203–214, Aug. 2019. https://doi.org/10.1016/j.cattod.2018.11.021

[8] Son I. H., Lee S. J., Song I. Y., Jeon W. S., Jung I., Yun D. J., Jeong D. W., Shim J. O., Jang W. J., and Roh H. S., Study on coke formation over $Ni/\gamma\text{-}Al_2O_3$, $Co\text{-}Ni/\gamma\text{-}Al_2O_3$, and $Mg\text{-}Co\text{-}Ni/\gamma\text{-}Al_2O_3$ catalysts for carbon dioxide reforming of methane, Fuel, vol. 136, pp. 194–200, Nov. 2014. https://doi.org/10.1016/j.fuel.2014.07.041

[9] R. Dębek, M. Motak, T. Grzybek, M. Galvez, and P. Da Costa, A short review on the catalytic activity of hydrotalcite-derived materials for dry reforming of methane, Catalysts, vol. 7, iss. 1, p. 32, Jan. 2017. https://doi.org/10.3390/catal7010032

[10] K. Y. Koo, H. S. Roh, Y. T. Seo, D. J. Seo, W. L. Yoon, and S. Bin Park, Coke study on MgO-promoted Ni/Al2O3 catalyst in combined H2O and CO2 reforming of methane for gas to liquid (GTL) process, Applied Catalysis A: General, vol. 340, iss. 2, pp. 183–190, Jun. 2008. https://doi.org/10.1016/j.apcata.2008.02.009

[11] M. Abbas, U. Sikander, M. T. Mehran, and S. H. Kim, Exceptional stability of hydrotalcite-derived spinel Mg(Ni)Al2O4 catalyst for dry reforming of methane, Catalysis Today, vol. 403, pp. 74–85, Nov. 2022. https://doi.org/10.1016/j.cattod.2021.08.029

[12] A. V. P. Lino, E. M. Assaf, and J. M. Assaf, Hydrotalcite-derived catalysts for syngas production from biogas reforming: Effect of nickel and cerium load, Catalysis Today, vol. 289, pp. 78–88, Jul. 2017. https://doi.org/10.1016/j.cattod.2016.08.022

[13] A. R. González, Y. J. O. Asencios, E. M. Assaf, and J. M. Assaf, Dry reforming of methane on Ni–Mg–Al nano-spheroid oxide catalysts prepared by the sol–gel method from hydrotalcite-like precursors, Applied Surface Science, vol. 280, pp. 876–887, Sep. 2013. https://doi.org/10.1016/j.apsusc.2013.05.082

[14] Gonzalez, S., Atia, H., Rockstroh, N., Lund, H., Bartling, S., Wohlrab, S., Armbruster, U., Impact of chelating agents on precursor formation and efficiency of Ni/MgO-Al2O3 catalysts in dry reforming of methane, Catalysis Today, vol. 429, Art. no. 114475, Mar. 2024. https://doi.org/10.1016/j.cattod.2023.114475

[15] J. Guo, H. Lou, H. Zhao, D. Chai, and X. Zheng, Dry reforming of methane over nickel catalysts supported on

magnesium aluminate spinels, Applied Catalysis A: General, vol. 273, no. 1–2, pp. 75–82, Oct. 2004. https://doi.org/10.1016/j.apcata.2004.06.014

[16] H. Özdemir, M. A. F. Öksüzömer, and M. A. Gürkaynak, Effect of the calcination temperature on Ni/$MgAl_2O_4$ catalyst structure and catalytic properties for partial oxidation of methane, Fuel, vol. 116, pp. 63–70, Jan. 2014. https://doi.org/10.1016/j.fuel.2013.07.095

[17] A. Valentini, N. L. V. Villarreal Carreño, L. F. D. Probst, P. N. Lisboa-Filho, W. H. Schreiner, E. R. Leite, and E. Longo, Role of vanadium in Ni: Ni:Al_2O_3 catalysts for carbon dioxide reforming of methane, Applied Catalysis A: General, vol. 255, iss. 2, pp. 211–220, Dec. 2003. https://doi.org/10.1016/S0926-860X(03)00560-X

[18] Yan Xu, Xi-hua Du, Jing Li, Peng Wang, Jing Zhu, Feng-jun Ge, Jun Zhou, Ming Song, and Wen-you Zhu, A comparison of Al2O3 and SiO2 supported Ni-based catalysts in their performance for the dry reforming of methane, Journal of Fuel Chemistry and Technology, vol. 47, iss. 2, pp. 199–208, Feb. 2019. https://doi.org/10.1016/S1872-5813(19)30010-6

[19] A. Sharma, I. Saito, H. Nakagawa, and K. Miura, Effect of carbonization temperature on the nickel crystallite size of a Ni/C catalyst for catalytic hydrothermal gasification of organic compounds, Fuel, vol. 86, no. 7–8, pp. 915–920, May 2007. https://doi.org/10.1016/j.fuel.2006.11.001